



Cite this: *Nanoscale*, 2016, **8**, 6456

Received 30th November 2015,
 Accepted 9th February 2016

DOI: 10.1039/c5nr08488a

www.rsc.org/nanoscale

Critical length scales and strain localization govern the mechanical performance of multi-layer graphene assemblies†

Wenjie Xia,^a Luis Ruiz,[‡] Nicola M. Pugno^{c,d,e} and Sinan Keten^{*a,b}

Multi-layer graphene assemblies (MLGs) or fibers with a staggered architecture exhibit high toughness and failure strain that surpass those of the constituent single sheets. However, how the architectural parameters such as the sheet overlap length affect these mechanical properties remains unknown due in part to the limitations of mechanical continuum models. By exploring the mechanics of MLG assemblies under tensile deformation using our established coarse-grained molecular modeling framework, we have identified three different critical interlayer overlap lengths controlling the strength, plastic stress, and toughness of MLGs, respectively. The shortest critical length scale L_c^s governs the strength of the assembly as predicted by the shear-lag model. The intermediate critical length L_c^p is associated with a dynamic frictional process that governs the strain localization propensity of the assembly, and hence the failure strain. The largest critical length scale L_c^t corresponds to the overlap length necessary to achieve 90% of the maximum theoretical toughness of the material. Our analyses provide the general guidelines for tuning the constitutive properties and toughness of multilayer 2D nanomaterials using elasticity, interlayer adhesion energy and geometry as molecular design parameters.

Graphene, one of the strongest materials known,^{1–3} is particularly suited for advanced structural and mechanical applications.^{4,5} In practice, its range of applications remains

limited due to the difficulty of harnessing the mechanical properties at larger length scales than those limited by the processing and synthesis of individual graphene sheets (in the order of nanometers to a few micrometers). In addition, its low extensibility and brittle failure behavior further restrict its usage in electronics, energy storage devices, and other applications where toughness and ductility are critical.

Drawing inspiration from biological architectures such as nacre, one possible way to simultaneously increase its extensibility and harness the properties of graphene in a scalable manner is to stack multiple sheets in a staggered fashion forming a so-called multi-layer graphene assembly (MLG).^{6–12} In materials with a multi-layer staggered architecture, the tensile load is transferred through shear at the interfaces and the deformation occurs by relative sliding between the sheets in different layers.¹³ For small deformations, where the sheet and interface behave linearly elastic to a good approximation, the continuum shear-lag model can be used to adequately predict the mechanical properties.^{14–17} However, as the deformation increases and more complex deformational mechanisms, such as strain localization, are activated, the shear-lag model breaks down. Understanding how architectural parameters, in particular the overlap length between the sheets in different layers, impact the mechanical behavior of the assembly is of critical importance for the rational design of optimal MLGs and other engineered 2D materials with an analogous architecture. Here, we use coarse-grained molecular dynamics (CG-MD) of MLGs under uniaxial tensile strain to identify the critical overlap length scales that control the strength, toughness and failure strain.

The CG molecular model of graphene used here (Fig. 1(a)) has been shown to accurately reproduce the elastic and fracture properties of single crystal graphene, as well as its interlayer shear behavior.¹⁸ Details of the CG force-field can be found in the original publication,¹⁸ and have also been included in the ESI,† together with a detailed presentation of the simulation parameters and protocols used in this work. We have simulated multiple MLG systems with a varying number of layers ($n_l = 2, 3, 5,$ and 10) and one sheet per layer ($n_s = 1$), which constitute a representative volume element

^aDepartment of Civil & Environmental Engineering, Northwestern University, 2145 Sheridan Road, Evanston, IL 60208, USA. E-mail: s-keten@northwestern.edu; Tel: +847-491-5282

^bDepartment of Mechanical Engineering, Northwestern University, 2145 Sheridan Road, Evanston, IL 60208, USA

^cDepartment of Civil, Environmental and Mechanical Engineering, Laboratory of Bio-inspired & Graphene Mechanics, University of Trento, Via Mesiano 77, 38123 Trento, Italy

^dCenter for Materials and Microsystems, Fondazione Bruno Kessler, Via Sommarive 18, 38123 Trento, Italy

^eSchool of Engineering and Materials Science, Queen Mary University of London, Mile End Road, London E1 4NS, UK

†Electronic supplementary information (ESI) available. See DOI: 10.1039/c5nr08488a

‡Current address: Chemical Sciences Division, Lawrence Berkeley National Laboratory, University of California, Berkeley, California 94720, USA.

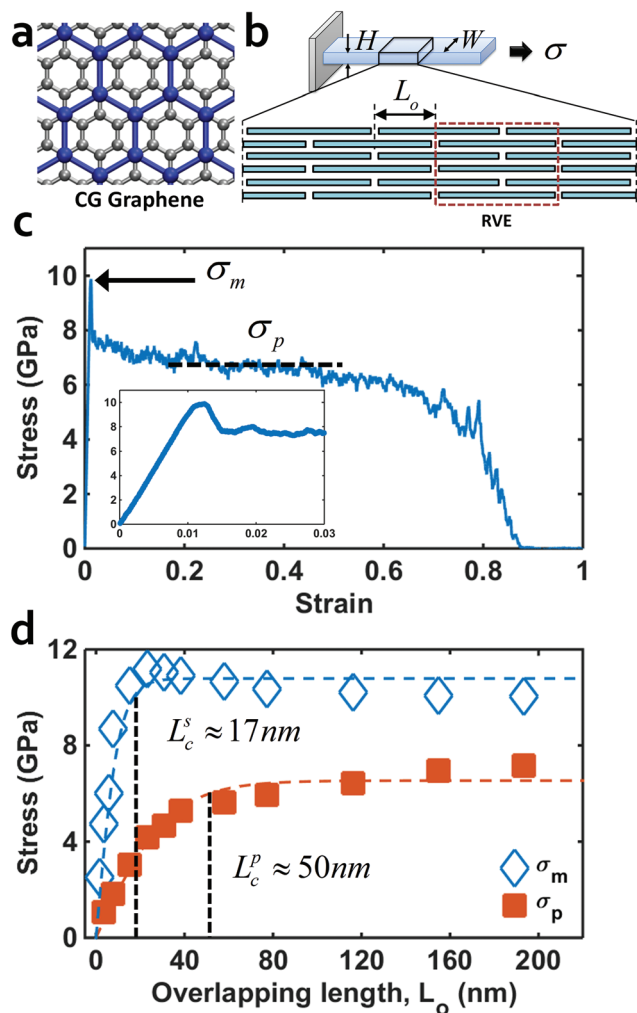


Fig. 1 (a) Mapping scheme from the atomistic lattice (gray) to the coarse-grained structure (blue). (b) Schematic of staggered multi-layer graphene (MLG) with an overlap length of L_o . (c) Typical stress–strain response of MLG with $L_o \sim 155$ nm under uniaxial tension. The inset highlights the linear elastic response at small strain. (d) The tensile strength σ_m and plastic stress σ_p of the MLG as a function of L_o . The dashed curves are the “shear-lag” model fits to the data. L_c^s and L_c^p are the critical overlap lengths for σ_m and σ_p , respectively, beyond which the σ_m and σ_p start to saturate.

(RVE) (Fig. 1(b)). The simulated MLGs in the RVE have overlap lengths L_o ranging from ~ 3 to 780 nm. The sheet’s width is set to be 6.4 nm for all the cases. Additional simulations are carried out and suggest that our results do not strongly depend on the sheet’s width. Each graphene sheet in the assembly is a single crystal without defects. We do not consider the grain boundary effects as the typical grain size of graphene ($\sim 10 \mu\text{m}$) is much larger than the sizes of our system.¹⁹ To verify that our findings are applicable to multiple sheets per layer, we also performed simulations for the $n_s = 3$ case. The results have been included in the ESI† and do not alter any of the conclusions presented. It is worth noting that the bonds of the CG model are breakable and that no further constraints are applied other than the imposed uniaxial strain,

i.e. we do not impose any a-priori failure or deformational mechanisms on the system.

The typical stress–strain response of MLGs exhibits a short linear elastic regime that ends with a sudden drop in the stress. A plastic regime follows the stress drop that ends in a rapid decay of the stress, which finally leads to failure (Fig. 1(c)). At the microscopic level, the fundamental deformational process of interlayer sliding is not continuum and consists of discrete transitions between the commensurate stacking configurations of graphene sheets in the neighboring layers (*i.e.* stick-slip mechanism). The elastic regime of the stress–strain response in this microscopic deformational picture corresponds to the period before the system undergoes the first slip event, which occurs within the range from $\sim 1\%$ to 4% strain depending on L_o for all the cases studied (inset of Fig. 1(c)). At these small deformations, the tensile stress of the MLGs results from static friction between van der Waals (vdW)-governed interfaces. Under these conditions, the Young’s modulus and the maximum stress σ_m , which we also refer to as the tensile strength here, can be predicted by the continuum shear-lag model:^{14,15}

$$\sigma_m = \frac{\sinh(L_o/l)\gamma_s^{cr}E_g h}{2(1 + \cosh(L_o/l)l)} \quad (1)$$

where $l = \sqrt{\frac{E_g h^2}{4G}}$ (≈ 5.2 nm) is a parameter that represents the length scale over which most of the stress is transferred in the interface, E_g (~ 950 GPa) is the Young’s modulus of graphene, G (~ 1 GPa) is the shear modulus of the interface, h ($= 3.35 \text{ \AA}$) is the equilibrium interlayer distance between the two layers, and γ_s^{cr} (~ 0.35) is the critical interlayer shear strain. The values of these fundamental parameters are set by the properties of the CG model, and thus they are not fitting parameters.¹⁸ The prediction of the MLG strength by the shear-lag model as a function of L_o is in very good agreement with the simulation results (Fig. 1(d)). Here, we define the critical length scale governing the strength of MLGs as L_o at which 90% of the maximum strength is achieved, and we obtain $L_c^s \sim 17$ nm, which is consistent with previous theoretical calculations that predicted $L_c^s \sim 3l$ for an analogous system.¹⁷ Although the maximum strength of MLGs (~ 10 GPa) is an order of magnitude lower than that of monocrystalline graphene (~ 100 GPa),¹ its strength still surpasses that of most structural engineered materials.

As previously mentioned, the elastic regime ends with a sudden drop in stress. We associate this drop to the transition from a static (before the first slip event) to a dynamic frictional situation^{20,21} (referred to here as the plastic regime because the deformations are irreversible). This drop after the peak stress could originate from the irregular stress distributions within the sheet, which will not strictly follow the shear-lag prediction. The plastic stress σ_p is defined as the average stress in the plateau plastic regime, which is indicated by the horizontal dashed lines in Fig. 1(c). Interestingly, the dependence of the post-peak plastic stress σ_p on L_o reveals that shear-lag scaling still holds (Fig. 1(d)). In fact, the trend can be quantitatively captured by eqn (1) if l (~ 16.3 nm) and γ_{cr} (~ 0.67)

are used as fitting parameters. This resulting weaker interface (*i.e.* softer and more ductile) in the plastic regime compared to the interface properties at small deformations is compatible with the static-to-dynamic frictional transition proposition. Similar to the critical length scale identified for the strength, we can define a second critical length scale associated with the saturation of the plastic stress to a near maximum value around $L_c^p \approx 50$ nm.

The physical meaning of L_c^p becomes clear when looking at the mechanical response of a single interface. Fig. 2(a) illustrates the bilayer model with a single interface used to characterize the constitutive force–displacement (f – u) response. To simplify our analysis, we apply the bilinear curve to characterize the f – u response (Fig. 2(b)). It can be observed that the nearly constant force regime lasts until the displacement u reaches $\sim(L_o - L_c^p)$, after which the force decays approximately linearly up to failure by a complete loss of overlap between the sheets. This analysis suggests that L_c^p is the critical overlap length after which the shear force at the interface does not depend on the overlap length. This observation can also be inferred from the shear-lag theory in which the strength σ_s and plastic stress σ_p are nearly independent of L_o as L_o is beyond L_c^s and L_c^p , respectively.

To be able to generalize these findings to other 2D materials, we need to understand the dependence of L_c^p on the constituent material properties, in particular the Young's modulus and interlayer adhesion energy. According to the shear-lag model,²² the critical length scale at which the tensile strength starts to saturate follows the scaling, $L_c^s \sim \sqrt{\frac{E_g}{G}}$. In the

stick-slip microscopic deformational mechanism, the shear rigidity depends linearly on the adhesion energy γ between the two sheets ($G \sim \gamma$). Therefore, from a theoretical standpoint, we expect L_c^p to follow a similar scaling, $L_c^p \sim \sqrt{\frac{E}{\gamma}}$. In fact, we find that the best fits to the simulation results $L_c^p \sim (E/E_g)^{0.41}$ and $L_c^p \sim 1/(\gamma/\gamma_g)^{0.52}$ (Fig. 3(a) and (b)) are in close agreement with the shear-lag exponent of 0.5. Although the particular value of L_c^p may also depend on other factors, such as the pulling velocity as in the case of atomic friction,^{21,23} we expect the scaling on constituent material properties to hold at a given rate.

Visualization of the simulation trajectories reveals that the deformation is uniformly distributed over all of the interfaces up to a certain point (the intermediate state), after which the strain localizes in a certain region along the length of the MLG (Fig. 4(a) and Movie S1†). The system ends up failing by deoverlapping in the region where the strain localizes. The deformation process identified from our simulations is schematically illustrated in Fig. 4(b). We characterize the intermediate state, or equivalently, the onset of localization by the displacement of each interface u_{int} at that moment. After the intermediate state, the strain localizes only on one side that keeps deoverlapping until failure. Using simple geometric argu-

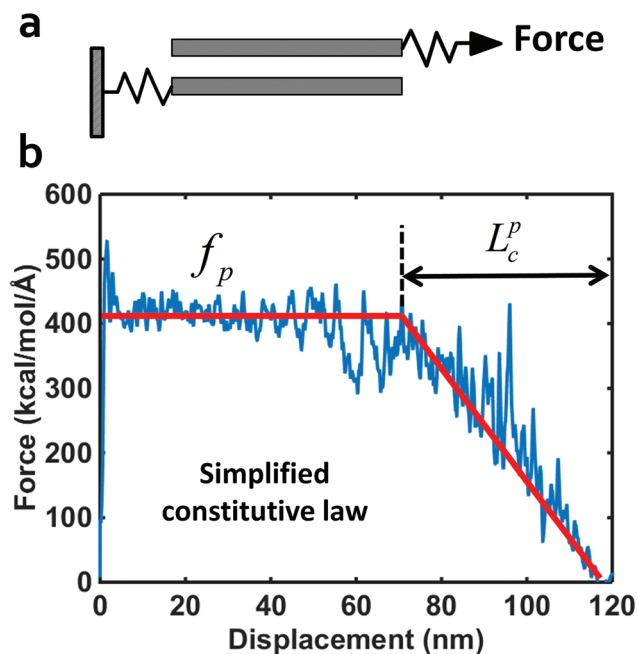


Fig. 2 (a) Schematic of a simplified bilayer model used to quantify the constitutive behavior of graphene with single interface. (b) Force–displacement (f – u) curve obtained from the pulling test. The resultant simplified constitutive law consists of a plateau force f_p regime and a linear decay regime as the remaining contact length is less than L_c^p , which is denoted by the bilinear solid lines.

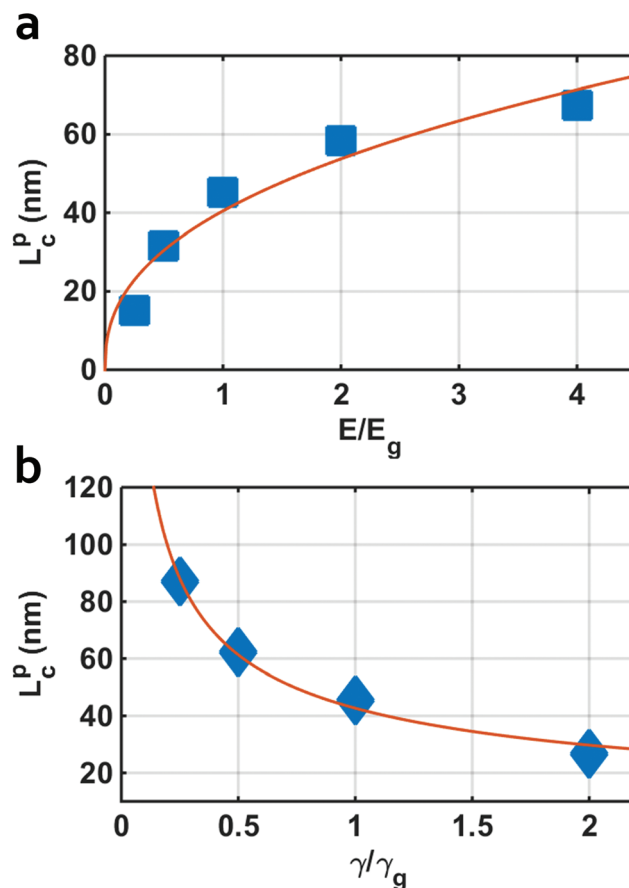


Fig. 3 Dependence of the critical length L_c on (a) sheet stiffness E and (b) interlayer adhesion energy γ determined from the pulling test of the bilayer model.

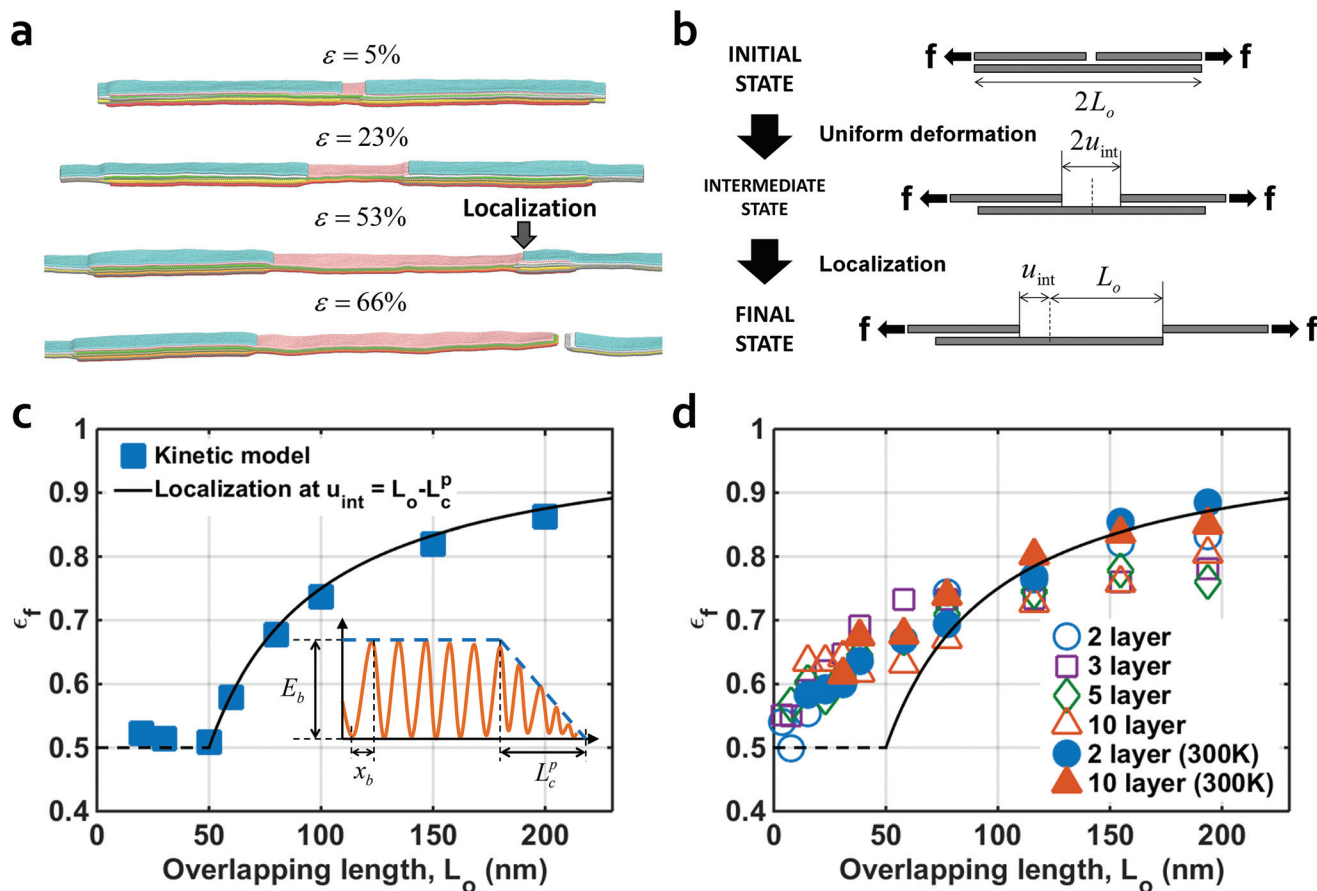


Fig. 4 (a) MD snapshots of the MLG deformation process. (b) Schematic of the sequence of different states during the deformation process. (c) Kinetic model prediction and (d) the MD simulation results of failure strain ϵ_f as a function of overlap length L_o . The inset of (c) shows the schematic of energy landscape used to predict strain localization in the simplest bilayer system. The solid curves in (c) and (d) show the failure strain prediction by assuming that the localization occurs when the remaining contact length of each part reduces to L_c^p .

ments, one can show that if localization occurs irreversibly at u_{int} , the failure strain ϵ_f is directly related to u_{int} *via*:

$$\epsilon_f = \frac{u_{\text{int}}}{2L_o} + \frac{1}{2} \quad (2)$$

or more generally for n_s sheets per layer,

$$\epsilon_f = \frac{(2n_s - 1)u_{\text{int}}}{2n_s L_o} + \frac{1}{2n_s} \quad (3)$$

In order to predict the failure strain of the MLG, we need to know when strain localization occurs, or equivalently, the value of u_{int} . Shearing of an interface proceeds through a series of slips between the equilibrium energy states where the lattices are in commensurate positions. Thus, we can think of interlayer sliding as a series of thermally activated jumps over energy barriers^{24,25} and use a kinetic model based on Bell's theory^{26–28} to describe the shear behavior of each interface. The lifetime τ of a single jump under an applied force is given by: $\tau = \exp\left(\frac{E_b - x_b f}{k_B T}\right) / \omega_0$, where ω_0 ($\sim 1 \times 10^{13} \text{ s}^{-1}$) is the vibrational frequency of the interface in the energy well,²⁶ $k_B T$ is the thermal energy, and x_b is the distance from equilibrium

to the transition state, which depends on the lattice spacing. The probability P_{over} of overcoming an energy barrier and advancing the system to the next equilibrium state (*i.e.* slipping) within a time interval Δt can therefore be approximated by: $P_{\text{over}} = 1 - \exp\left(-\frac{\Delta t}{\tau}\right)$. Using this theoretical scheme, we can numerically simulate the deformation of two interfaces and measure u_{int} , which would correspond to the displacement at which one of the interfaces gets trapped in a local minimum while the other keeps sliding under the applied force. A detailed description of this kinetic model is given in the ESI.† The results of this model reveal that strain localization always initiates when the displacement is $u_{\text{int}} = L_o - L_c^p$ for $L_o > L_c^p$. This finding suggests that L_c^p is a critical length which is also associated with strain localization, and hence failure strain. Substituting $u_{\text{int}} = L_o - L_c^p$ into eqn (2), ϵ_f can be directly expressed as:

$$\epsilon_f = 1 - \frac{L_c^p}{2L_o} \quad (4)$$

This equation accurately captures the ϵ_f obtained from the kinetic model analysis (Fig. 4(c)). When $L_o < L_c^p$, the kinetic

model predicts that localization initiates from the start of the deformation, which leads to $\varepsilon_f \sim 0.5$. It is worth noting that the minimum and maximum theoretical failure strain in this system ($n_s = 1$) is 0.5 and 1, respectively. The predictions of the kinetic model agree well with what is observed in the CG-MD simulations for $L_o > L_c^p$ (Fig. 4(d)), suggesting that the origin of the strain localization is kinetic trapping of one of the interfaces in a local energy minimum. For $L_o < L_c^p$, the CG-MD simulations show slightly greater failure strains than the kinetic model predictions, which we attribute to the fact that at a finite rate and short L_o , some homogeneous deformation can still carry on before strain localization occurs. It should be noted that changing the x_b of the CG model (~ 0.2 nm) to the value of atomistic graphene (~ 0.1 nm) will not change the kinetic model predictions.

Once we are able to theoretically predict the plastic stress and the failure strain of MLGs, we can attempt to predict the toughness of the system, or equivalently, its energy dissipation capacity, defined as the area under the stress-strain curve. If we follow the definition of toughness and simplify the stress-strain response as a constant plateau at σ_p followed by a linear decay after strain localization, the toughness T can be directly approximated by a simple expression:

$$T = \int_0^{\varepsilon_f} \sigma d\varepsilon = \sigma_p \left(1 - \frac{L_c^p}{L_o} \right) + \frac{\sigma_p L_c^p}{4n_s L_o} \quad (5)$$

The quantitative agreement between this relationship and the toughness from the simulations is remarkable considering the simplicity of the model (Fig. 5(a)). Notably, eqn (5) implies that the toughness of MLG saturates at large L_o . Defining the critical length L_c^T as before following the 90% criteria, we get $L_c^T \approx 400$ nm or $\sim 8L_c^p$ for $n_s = 1$. Further increase in L_o beyond this critical length will not enhance the toughness significantly. This critical overlap length L_c^T is an extremely relevant design guideline for the design of tough MLG papers. Our simulations show that the theoretical maximum toughness

($\sim 7 \times 10^3$ MJ m⁻³) or specific energy dissipation ($E_p^* \sim 3$ MJ kg⁻¹) that can be achieved by the MLG is roughly an order of magnitude higher compared to other engineering materials, such as steel and Kevlar armor.^{19,29,30} Our simulations also suggest that the theoretical maximum toughness values are much higher than those recently measured by supersonic ballistic experiments on MLGs ($E_p^* \sim 1.5$ MJ kg⁻¹).¹⁹

It is important to note that the energy of the intralayer interactions (*i.e.* interactions between different sheets in the same layer) is negligible compared to the surface energy between the sheets in different layers. This is because within each layer, the side-by-side interaction energy of the graphene sheets is much smaller than the strength of the covalent bonds within each sheet, and thus its contribution to features such as modulus and strength is negligible. The tensile load in the MLGs is transferred through shear between sheets in different layers rather than through serial force transfer between the sheets in the same layer. Accordingly, we have not included these edge effects in the analysis presented above. Also, although we have considered only monocrystalline graphene for our sheets, the presence of grain boundaries will most likely not change our results, as the energy to break those bonds will be much larger than the shear barriers imposed by the weak van der Waals interactions, maintaining the failure mode by deoverlapping unchanged. These assumptions will need to be revisited if the system under study includes cross-links that strengthen the intralayer interactions or the interfaces.

Our findings provide several strategies for improving toughness. First, given that L_c^T is directly related to L_c^p , the failure strain and toughness can be controlled by tuning the stiffness E of the constituent sheets and the interfacial adhesion energy γ between the sheets by functionalizing the surface. The prediction of L_c^T as a function of E and γ is shown in Fig. 5(b). There are various pathways through which these material properties could be tailored. For example, by oxidizing the carbon

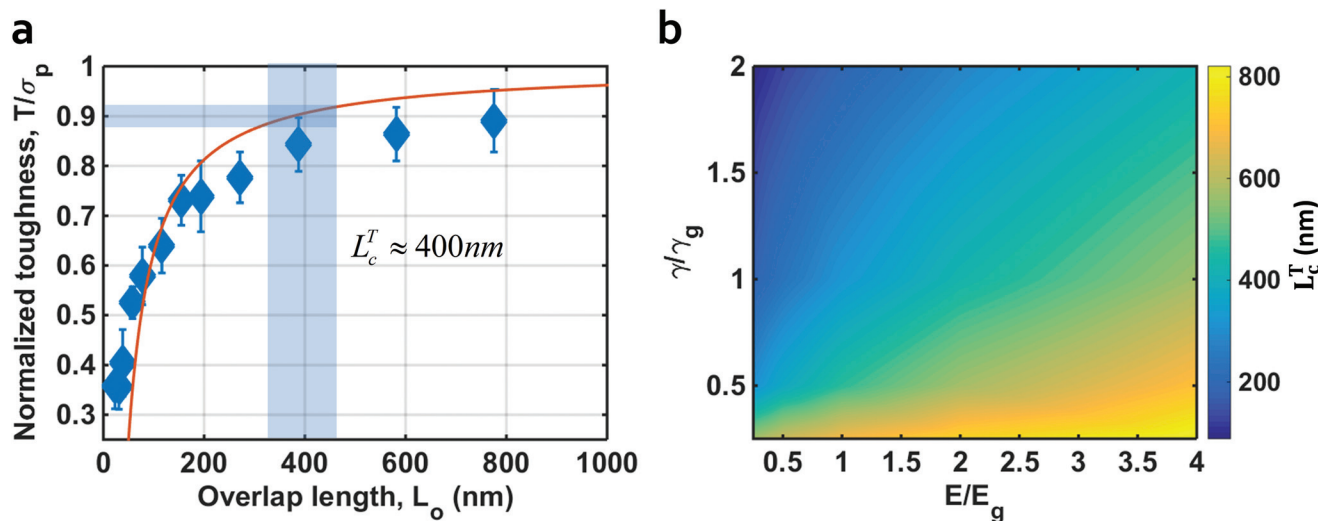


Fig. 5 (a) Normalized toughness T/σ_p as a function of overlap length. The solid curve shows the prediction from eqn (5) for $n_s = 1$. (b) The predicted critical length L_c^T for the toughness as a function of sheet stiffness E and interlayer adhesion energy γ .

atoms at different functionalization levels (the fraction of oxidized carbon atoms), forming the so-called graphene oxide (GO) paper, the enhanced interfacial adhesion energy and reduced modulus compared to pristine graphene can be utilized to design these length scale parameters and thus material toughness.^{4,31} Second, the interlayer shear response of graphene, such as shear modulus, interaction energy, and frictional force, depends on the stacking orientation due to the hexagonal lattice feature,^{18,32,33} and thus it would be expected that L_c^P and L_c^T also vary for different stacking orders (e.g. Bernal vs. turbostratic). The scaling relationship between L_c^P and factors such as stiffness and adhesion energy can be readily used to predict L_c^T for different stacking orientations. Such predictions may enable the design of tougher protection materials using MLG, since recent projectile penetration experiments have already shown multilayer graphene to be excellent for this purpose due to its superior energy absorption capacity.¹⁹ Our findings on mechanical behaviors of MLG with a staggered architecture can be applied to design materials with dramatically enhanced toughness and energy adsorption. Moreover, our results of the size-dependent mechanical response and failure mechanism of MLG can be adapted to other 2D materials whose interfacial properties are governed by vdW interactions as well, such as phosphorene, MoS₂ and hBN.^{34–37} For instance, for the case of phosphorene which has a rougher potential energy landscape and a lower sheet stiffness compared to graphene, its L_c^T of a multilayer system will be smaller than that of graphene based on our predictions as shown in Fig. 5(b). Future work on theoretical description of plastic stress associated with the dynamic friction process will be a key to quantitatively predict the mechanical responses of multilayer assemblies of 2D nanomaterials in large deformation regimes.

Conclusions

In summary, we have performed CG-MD simulations to provide unprecedented quantitative understanding of the dependence of the mechanical properties of MLG on the interlayer overlap length L_o , including the elusive large deformation and failure regimes where continuum models often break down. We have developed analytical expressions for a hierarchy of critical overlap lengths that govern the strength ($L_c^S \sim 17$ nm), failure strain and plastic stress ($L_c^P \sim 50$ nm), and the toughness ($L_c^T \sim 400$ nm) of MLGs. Particularly interesting, we found that the toughness of MLGs does not significantly increase with the overlap length for a very large L_o beyond $\sim L_c^T$. In fact, 90% of the maximum theoretical toughness can be already achieved for the overlap lengths $\sim L_c^T$, which can be considered as an extremely important design parameter to design tough multilayer graphene systems. More importantly, we have elucidated the functional dependence of these critical length scales with the mechanical properties of the constituent materials, thus providing transferrable guidelines to assemblies with similar multi-layered staggered architectures based

on 2D materials with different interfacial or elastic properties, such as phosphorene, MoS₂ and hBN.

Acknowledgements

The work is funded by the National Science Foundation (DMREF award CMMI-1235480). The authors acknowledge the support from the Departments of Civil and Environmental Engineering and Mechanical Engineering at Northwestern University, as well as the Northwestern University High Performance Computing Center for a supercomputing grant. N.M.P. is supported by the European Research Council (ERC StG Ideas 2011 BIHSNAM no. 279985 on 'Bio-Inspired hierarchical super-nanomaterials', ERC PoC 2015 SILKENE no. 693670 on 'Bionic silk with graphene or other nanomaterials spun by silkworms', ERC PoC 2013-2 KNOTOUGH no. 632277 on 'Super-tough knotted fibres') by the European Commission under the Graphene Flagship (WP10 'Nanocomposites', no. 604391) and by the Provincia Autonoma di Trento ('Graphene Nanocomposites', no. S116/2012-242637 and reg.delib. no. 2266). We thank our collaborators Horacio Espinosa, SonBinh T. Nguyen and Jeff Paci for fruitful discussions on the mechanics and computational modeling of multi-layer graphene.

References

- 1 C. Lee, X. D. Wei, J. W. Kysar and J. Hone, *Science*, 2008, **321**, 385–388.
- 2 C. Lee, X. D. Wei, Q. Y. Li, R. Carpick, J. W. Kysar and J. Hone, *Phys. Status Solidi B*, 2009, **246**, 2562–2567.
- 3 F. Liu, P. M. Ming and J. Li, *Phys. Rev. B: Condens. Matter*, 2007, **76**, 064120.
- 4 Y. W. Zhu, S. Murali, W. W. Cai, X. S. Li, J. W. Suk, J. R. Potts and R. S. Ruoff, *Adv. Mater.*, 2010, **22**, 3906–3924.
- 5 R. J. Young, I. A. Kinloch, L. Gong and K. S. Novoselov, *Compos. Sci. Technol.*, 2012, **72**, 1459–1476.
- 6 M. J. Buehler, *Proc. Natl. Acad. Sci. U. S. A.*, 2006, **103**, 12285–12290.
- 7 H. D. Espinosa, J. E. Rim, F. Barthelat and M. J. Buehler, *Prog. Mater. Sci.*, 2009, **54**, 1059–1100.
- 8 P. Egan, R. Sinko, P. R. LeDuc and S. Keten, *Nat. Commun.*, 2015, **6**, 1–12.
- 9 H. Chen, M. B. Muller, K. J. Gilmore, G. G. Wallace and D. Li, *Adv. Mater.*, 2008, **20**, 3557–3561.
- 10 O. C. Compton and S. T. Nguyen, *Small*, 2010, **6**, 711–723.
- 11 D. Li, M. B. Muller, S. Gilje, R. B. Kaner and G. G. Wallace, *Nat. Nanotechnol.*, 2008, **3**, 101–105.
- 12 C. Shao and S. Keten, *Sci. Rep.*, 2015, **5**, 16452.
- 13 B. H. Ji and H. J. Gao, *Annu. Rev. Mater. Res.*, 2010, **40**, 77–100.
- 14 H. L. Cox, *Br. J. Appl. Phys.*, 1952, **3**, 72–79.
- 15 B. Chen, P. D. Wu and H. Gao, *Compos. Sci. Technol.*, 2009, **69**, 1160–1164.

- 16 X. D. Wei, M. Naraghi and H. D. Espinosa, *ACS Nano*, 2012, **6**, 2333–2344.
- 17 Y. Liu, B. Xie, Z. Zhang, Q. Zheng and Z. Xu, *J. Mech. Phys. Solids*, 2012, **60**, 591–605.
- 18 L. Ruiz, W. J. Xia, Z. X. Meng and S. Keten, *Carbon*, 2015, **82**, 103–115.
- 19 J.-H. Lee, P. E. Loya, J. Lou and E. L. Thomas, *Science*, 2014, **346**, 1092–1096.
- 20 B. N. Persson, *Sliding friction: physical principles and applications*, Springer Science & Business Media, 2000.
- 21 H. Hölscher, A. Schirmeisen and U. D. Schwarz, *Philos. Trans. R. Soc., A*, 2008, **366**, 1383–1404.
- 22 N. Pugno, Q. Yin, X. Shi and R. Capozza, *Meccanica*, 2013, **48**, 1845–1851.
- 23 O. Zworner, H. Holscher, U. D. Schwarz and R. Wiesendanger, *Appl. Phys. A: Mater. Sci. Process.*, 1998, **66**, S263–S267.
- 24 G. A. Tomlinson, *Philos. Mag.*, 1929, **7**, 905–939.
- 25 L. Prandtl, *Z. Angew. Math. Mech.*, 1928, **8**, 85–106.
- 26 G. Bell, *Science*, 1978, **200**, 618–627.
- 27 S. Keten and M. J. Buehler, *Phys. Rev. E: Stat., Nonlinear, Soft Matter Phys.*, 2008, **78**.
- 28 S. Keten and M. J. Buehler, *Nano Lett.*, 2008, **8**, 743–748.
- 29 J. Dean, C. S. Dunleavy, P. M. Brown and T. W. Clyne, *Int. J. Impact Eng.*, 2009, **36**, 1250–1258.
- 30 B. L. Lee, T. F. Walsh, S. T. Won, H. M. Patts, J. W. Song and A. H. Mayer, *J. Compos. Mater.*, 2001, **35**, 1605–1633.
- 31 D. A. Dikin, S. Stankovich, E. J. Zimney, R. D. Piner, G. H. B. Dommett, G. Evmenenko, S. T. Nguyen and R. S. Ruoff, *Nature*, 2007, **448**, 457–460.
- 32 M. Dienwiebel, G. S. Verhoeven, N. Pradeep, J. W. M. Frenken, J. A. Heimberg and H. W. Zandbergen, *Phys. Rev. Lett.*, 2004, **92**.
- 33 I. V. Lebedeva, A. A. Knizhnik, A. M. Popov, Y. E. Lozovik and B. V. Potapkin, *Phys. Chem. Chem. Phys.*, 2011, **13**, 5687–5695.
- 34 Q. Wei and X. Peng, *Appl. Phys. Lett.*, 2014, **104**, 251915.
- 35 K. S. Novoselov, D. Jiang, F. Schedin, T. J. Booth, V. V. Khotkevich, S. V. Morozov and A. K. Geim, *Proc. Natl. Acad. Sci. U. S. A.*, 2005, **102**, 10451–10453.
- 36 C. Lee, Q. Y. Li, W. Kalb, X. Z. Liu, H. Berger, R. W. Carpick and J. Hone, *Science*, 2010, **328**, 76–80.
- 37 A. K. Geim and I. V. Grigorieva, *Nature*, 2013, **499**, 419–425.

Supporting Information for

Critical length scales and strain localization govern the mechanical performance of multi-layer graphene assemblies

Wenjie Xia, Luis Ruiz, Nicola M. Pugno, Sinan Keten *

Department of Civil and Environmental Engineering and Department of Mechanical Engineering,
Northwestern University, 2145 Sheridan Road, Evanston, IL, 60208

*Corresponding Author: s-keten@northwestern.edu

Overview of coarse-grained (CG) graphene model

The coarse-grained (CG) model follows a 4-to-1 mapping scheme, where 4 carbon atoms are represented by 1 CG bead. The hexagonal symmetry of the atomic lattice is conserved to capture the interlayer shear response, including superlubricity effects. The CG force-field was developed based on a strain energy conservation approach, and it includes bonded contributions from bonds V_b , angles V_a , and dihedrals V_d , and nonbonded contributions from the interlayer interactions V_{nb} . There is no nonbonded interaction between CG atoms within each sheet. The force-field parameters (Table S1) are calibrated using mechanical properties obtained from density functional theory and experiments, such as elastic tensile and shear modulus, and the failure properties. The developed CG model allows us to simulate large multi-layer graphene (MLG) systems with a ~200 fold increase in computational speed in comparison with all-atomistic simulations. The detailed derivation of the force field parameters can be found in our earlier work [1].

It should be noted that the interlayer shear modulus G determined from the bilayer shear test in our previous work is reported to be ~2 GPa, which is determined from the maximum slope in the shear force-displacement curve [1]. However, the actual shear response is not perfectly linear

due to the van der Waals interlayer interactions. In our current study, we use $G \sim 1$ GPa by linearizing the force-displacement response, which can be considered as the averaged shear modulus. Additionally, it has been well accepted that the Young's modulus of monolayer graphene sheet E_g is derived based on the definition of monolayer graphene thickness of $h = 3.35 \text{ \AA}$, which is equivalent to the 2D modulus (D) defined as $D = E_g h$ [2]. We choose the former modulus definition in this study. Also note that the exact form of conventional shear-lag equation used to predict the "mortar-brick" system is slightly different from Eq. (1) due to the thickness definition of monolayer graphene. To apply the shear-lag model to MLGs, the 2D modulus (D) as $D = E_g h$ is usually employed to avoid the issue of thickness definition of each graphene sheet.

Table S1. Summary of Functional Forms and Calibrated Parameters of the Coarse-grain Graphene Model Force Field.

Interaction	Functional Form	Parameters
Bond	$V_b(d) = D_0 \left[1 - e^{-\alpha(d-d_0)} \right]^2$ for $d < d_{cut}$	$d_0 = 2.8 \text{ \AA}$
		$D_0 = 196.38 \text{ kcal / mol}$
		$\alpha = 1.55 \text{ \AA}^{-1}$
		$d_{cut} = 3.49 \text{ \AA}$
Angle	$V_a(\theta) = k_\theta (\theta - \theta_0)^2$	$\theta_0 = 120^\circ$
		$k_\theta = 409.40 \text{ kcal / mol}$
Dihedral	$V_d(\varphi) = k_\varphi [1 - \cos(2\varphi)]$	$k_\varphi = 4.15 \text{ kcal / mol}$
Non-bonded	$V_{nb}(r) = 4\epsilon_g \left[\left(\frac{\sigma}{r} \right)^{12} - \left(\frac{\sigma}{r} \right)^6 \right]$ for $r < r_{cut}$	$\sigma = 3.46 \text{ \AA}$
		$\epsilon_g = 0.82 \text{ kcal / mol}$
		$r_{cut} = 12 \text{ \AA}$

Characterization of single interface in a bilayer system

To understand the interlayer shear response in detail, we study a single interface (illustrated in Fig. 2(a)). This system is often considered as a basic representative volume element (RVE) in the shear-lag model based on continuum analysis [3-5]. The interlayer shear behavior of graphene

sheets is investigated by means of steered molecular dynamics (SMD) simulations [6] using the LAMMPS package [7].

In the SMD simulations, the left end of the bottom sheet is fixed, and the right end of the top one is pulled in the longitudinal direction by applying a force f generated by a stiff harmonic spring:

$$f = k_{SMD}(vt - x(t)) \quad (S1)$$

where k_{SMD} is the spring constant and v is the pulling velocity. A relatively stiff spring constant of 1000 kcal/mol Å² and a pulling velocity of 0.0005 Å/fs that is the same with the displacement rate of multi-layer graphene are chosen for the SMD simulations. The spring constant adopted herein has been shown in previous studies to be a reasonable choice leading to independence of the measured mechanical properties from the spring constant [1,8]. The pulling velocity also lies in the conventional strain rate regime ($\sim 10^7$ to 10^9 s⁻¹) as commonly used in molecular dynamics studies [9-11]. The sheet length (or overlap length) is ~ 116 nm, which is well beyond the critical lengths identified from the strength and plastic stress of multi-layer graphene (L_c^s and L_c^p shown in Fig. 1(d)). The system is first relaxed through the energy minimization and dynamics run for 5000 time steps with a time step of 4 fs. After equilibration, the SMD simulation is performed at 10 K under an NVT ensemble (thermodynamic ensemble with constant number of particles, volume, and temperature). The resultant force-displacement curve can be simply described by the bilinear curves that consist of a plateau force f_p region and a linear decay region (as shown in Fig. 2(b)). The length of the linear stress decay region coincides with the critical length of L_c^p from the plastic stress measurement.

Description of the kinetic model used to characterize strain localization

To understand the failure behavior and strain localization mechanism of MLG, we employ the kinetic model on the basis of thermally activated process as observed in the atomic friction phenomenon. The representative volume element (RVE) system that we numerically simulate is equivalent to a MLG with 2 layers and 1 flake per layer ($n_l = 2$ and $n_s = 1$) with periodic boundary conditions in the longitudinal direction (x-direction). The simplification process that we follow to model the system for the kinetic model is illustrated in Fig. S1. The system is composed of two 1D energy landscapes, each representing one of the graphene-graphene interfaces. The energy landscape of each interface consists of a series of energy barriers, where the distance between two neighboring energy barriers is d_b , which is taken as the hexagonal lattice spacing of ~ 0.4 nm, and the distance from the well to the barrier is $x_b = d_b/2$. The shape of the energy landscape is constructed based on the constitutive shear responses of single interface characterized by the SMD simulations (force-displacement curve shown in Fig. 2(b) in main text). The height of the energy barriers E_b from $x = 0$ to $x = L_o - L_c^p$ is constant and can be approximated as $E_b \approx f_p \cdot x_b \approx 800$ kcal/mol. From the downturn point ($x = L_o - L_c^p$), the magnitude of the barriers decays linearly up to $x = L_o$.

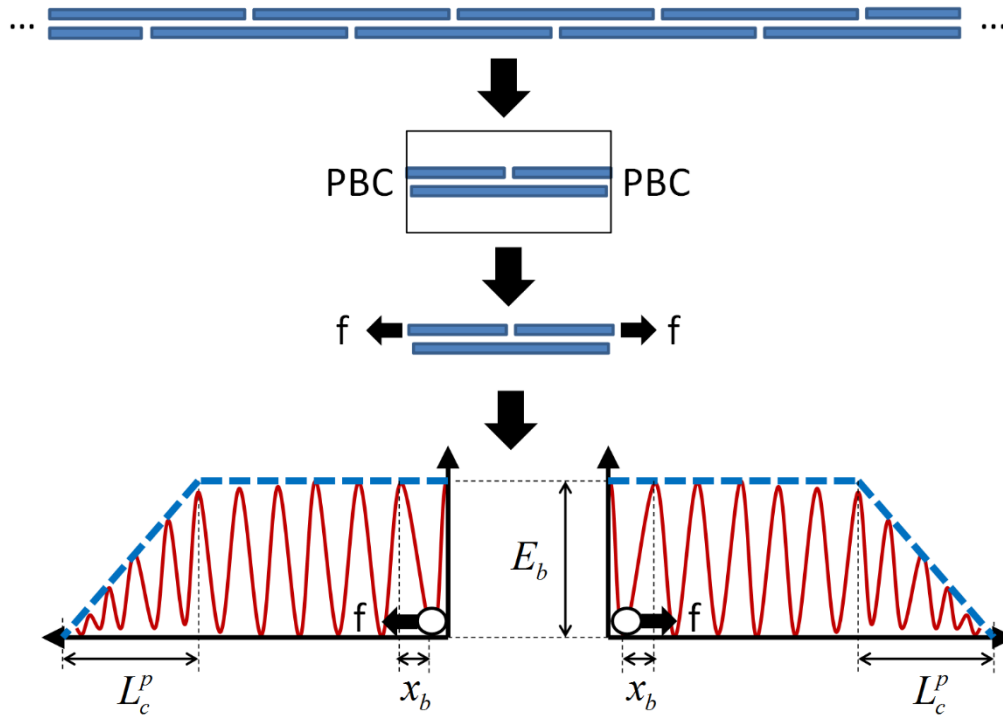


Figure S1. Illustration of the kinetic model in the representative volume element (RVE) bilayer system with two interfaces. The energy landscape of each interface is illustrated on the bottom, in which E_b is the energy barrier and x_b is half of the distance between the two neighboring barriers.

The inputs for the model are the overlap length L_o (i.e. length of each interface), the critical length L_c^p , the distance between energy barriers d_b , the thermal energy $k_B T$, the magnitude of the energy barriers E_b , and the vibrational frequency of the interface in the energy well ω_0 . The output of each simulation is the failure strain of the system ε_f .

The numerical simulation proceeds as follows. At a given step, we apply a force f to both interfaces and calculate the probability of each one overcoming the energy barrier. According to

Bell's theory [12], the life time τ of each jump between equilibrium states under an applied force can be calculated as:

$$\tau = \exp\left(\frac{E_b - x_b f}{k_B T}\right) / \omega_0 \quad (\text{S2})$$

The probability of the graphene sheet at each interface overcoming the energy barrier within a time interval Δt can therefore be approximated by:

$$P_{over}^i = 1 - \exp\left(-\frac{\Delta t}{\tau}\right) \quad (\text{S3})$$

$$P_{over}^i = 1 - \exp\left[-\omega_0 \Delta t \exp\left(-\left(E_b^j - x_b f\right) / k_B T\right)\right] \quad (\text{S4})$$

The superscript $i = 1, 2$ stands for each of the two interfaces. The superscript j denotes the energy barrier number in the landscape that the interface is attempting to overcome. To decide if an interface jumps over the barrier to the next equilibrium state, we compare P_{over} to a random number with a uniform probability distribution between 0 and 1, and if $rand < P_{over}$, then that interface advances to the next equilibrium energy state. If neither of the interfaces overcomes the barrier, then the force is increased by Δf and whether the interfaces advance or not is checked again. If at least one of the interfaces advances to the next equilibrium state, then the position of that interface is updated and the previous steps are iterated. The simulation stops when one of the interfaces overcomes the last energy barrier at the fully separated state. For each set of input parameters, 1000 simulations are performed. The failure strain that we report (Fig. 4(c) in the main text) is calculated as the average of the results from those 1000 numerical simulations, and the standard deviations are within the data symbol size. The calculation protocol of the kinetic model used to characterize the failure of the MLG is summarized in the flowchart in Fig. S2.

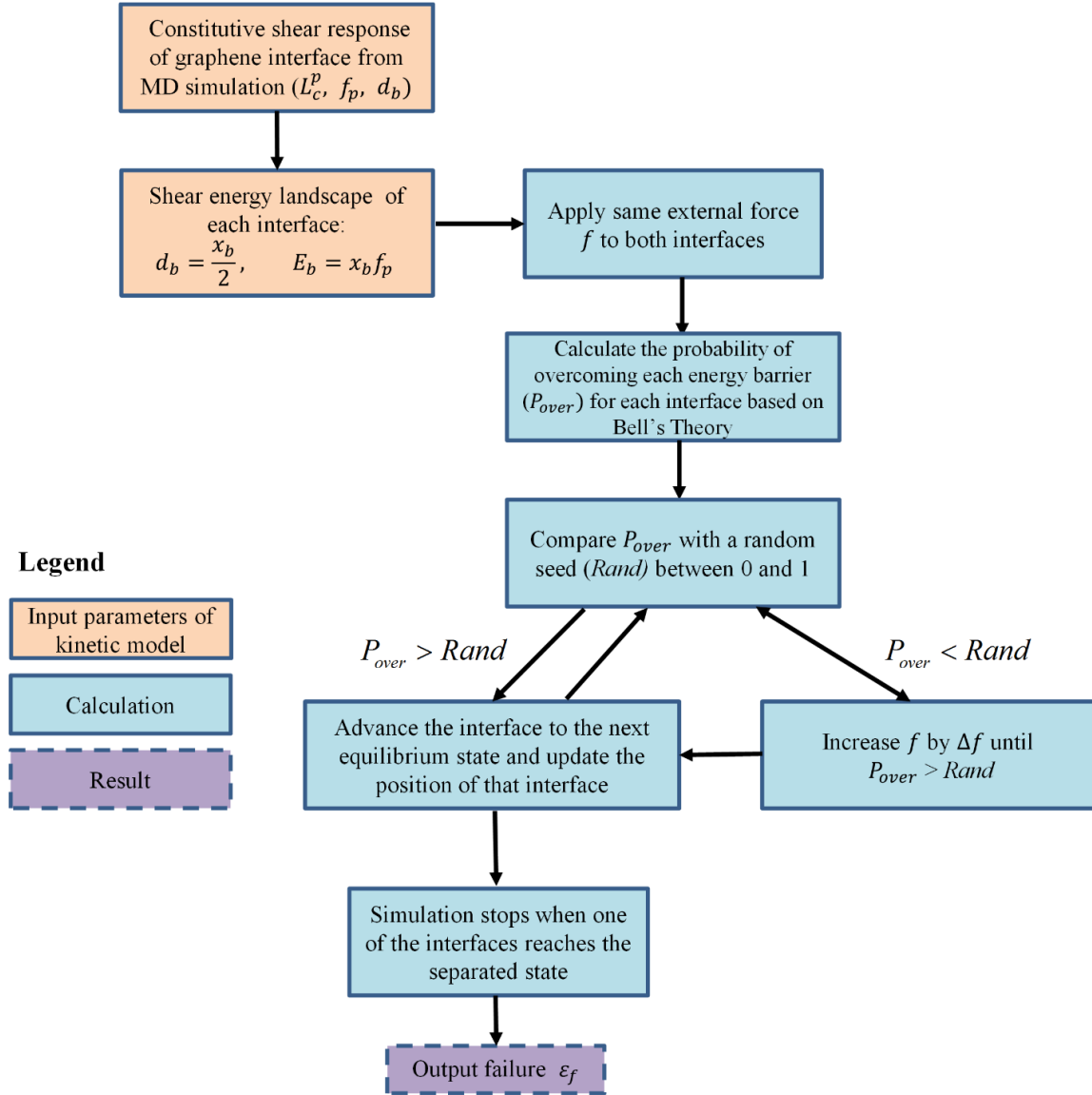


Figure S2. Flowchart that summarizes the calculation protocol of the kinetic model used to characterize the failure of the MLG.

In the model, we use $\omega_0 \sim 1 \times 10^{13}$ 1/s that is the typical natural frequency of oscillation of atoms in solids [12-14]. The time interval Δt to calculate P_{over} can be approximated as: $\Delta t \sim \frac{d_b}{v} \sim 1 \times 10^{-11}$ s. All the parameters used in the kinetic model prediction as reported in the main manuscript are summarized in Table S2. To make sure that the kinetic model makes

physical sense, we also perform sensitivity analysis of the failure strain as a function of parameters E_b and $\omega_0\Delta t$ in the kinetic model. The result of the sensitivity analysis as shown in Fig. S3 indicates that the predicted failure strain from the kinetic model is nearly independent of these system parameters within the reasonable range. Note that changing $d_b \sim 0.4$ nm to ~ 0.2 nm based on the atomistic graphene lattice spacing will not change the kinetic model predictions.

Table S2. Summary of the Parameters of the Kinetic Model used in the Main Manuscript.

Variable/symbol	Parameters
E_b	800 kcal/mol
d_b	0.4 nm
ω_0	$1 \times 10^{13} \text{ s}^{-1}$
Δt	$1 \times 10^{-11} \text{ s}$
$k_B T$	0.593 kcal/mol
L_c^p	50 nm

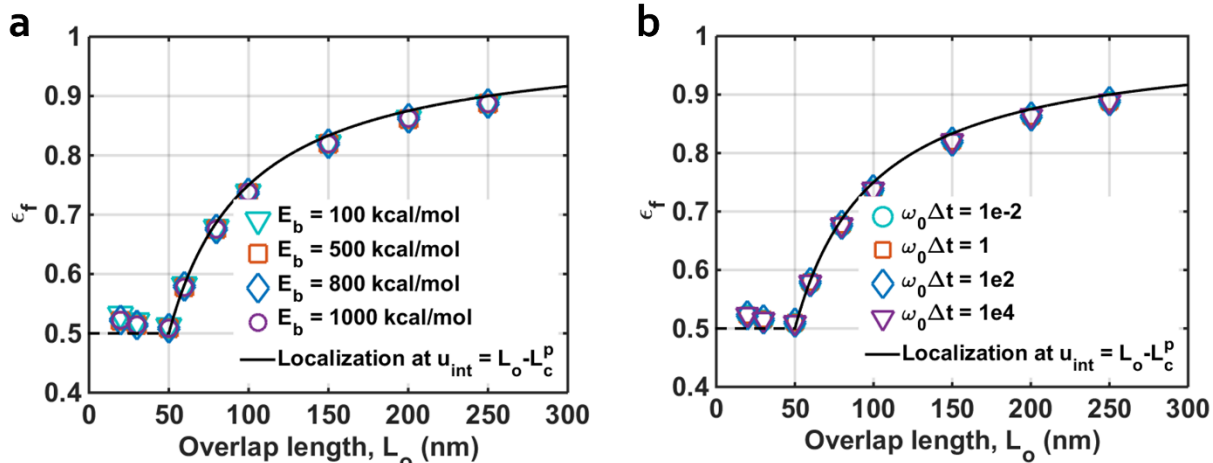


Figure S3. Sensitivity analysis for failure strain ϵ_f prediction as a function of the parameters (a) E_b and (b) $\omega_0 \Delta t$ used in the kinetic model. The result indicates that predicted failure strain from the kinetic model is nearly independent of these system parameters within the reasonable range.

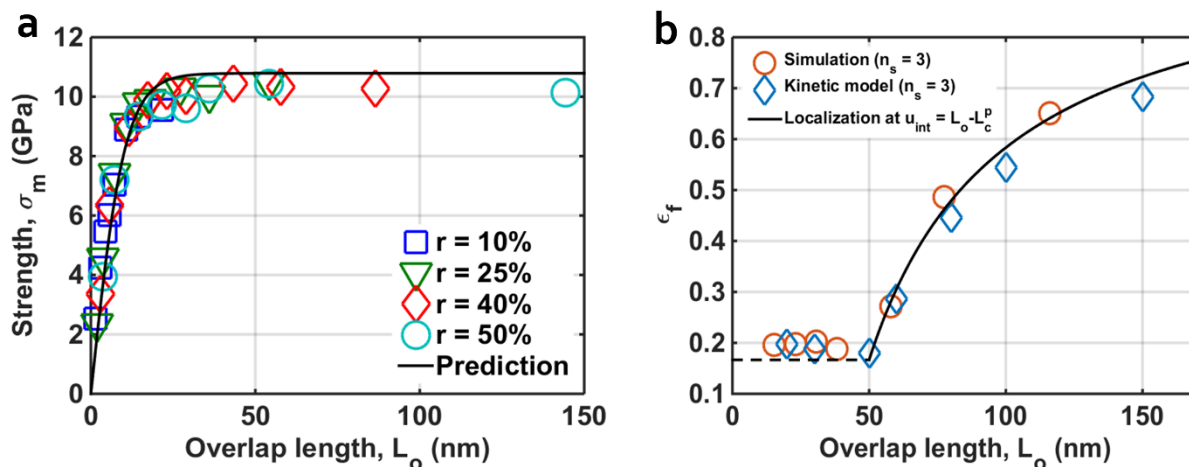


Figure S4. (a) The tensile strength σ_m with different overlap ratio r and (b) failure strain ϵ_f as a function of overlap length for the MLG with 3 sheets per layer ($n_s = 3$).

The analysis of kinetic model indicates that the strain localization always initiates at the displacement around $u_{int} = L_o - L_c^p$, when $L_o > L_c^p$, leading to the failure strain $\epsilon_f = 1 - \frac{L_c^p}{2L_o}$. We perform additional simulations and kinetic analysis for the case with three sheets per layer ($n_s =$

3) to verify our results. The tensile strength σ_m for the MLG with $n_s = 3$ and different overlap ratio r shows indistinguishable difference from the case $n_s = 1$ (Fig. S4(a)). The prediction of ε_f from the kinetic model agrees well with our CG-MD simulations as shown in Fig. S4(b).

Knowing the failure strain, the toughness T of the bilayer system with two interfaces ($n_s = 1$) can be directly approximated by integrating the stress-strain curve:

$$T = \int_0^{\varepsilon_f} \sigma d\varepsilon = \sigma_p \left(\frac{2L_o - 2L_c^p}{2L_o} \right) + \frac{1}{2} \frac{\sigma_p L_c^p}{L_o} = \sigma_p \left(1 - \frac{L_c^p}{L_o} \right) + \frac{\sigma_p L_c^p}{4L_o} \quad (\text{S5})$$

The above equation can be generalized for n_s number of flakes per layer, leading to Eq. (S6) (corresponding to the Eq. (5) in the main manuscript):

$$T = \sigma_p \left(\frac{2n_s L_o - 2n_s L_c^p}{2n_s L_o} \right) + \frac{1}{2} \frac{\sigma_p L_c^p}{2n_s L_o} = \sigma_p \left(1 - \frac{L_c^p}{L_o} \right) + \frac{\sigma_p L_c^p}{4n_s L_o} \quad (\text{S6})$$

REFERENCES

- [1] L. Ruiz, W. J. Xia, Z. X. Meng, and S. Keten, Carbon **82**, 103 (2015).
- [2] C. Lee, X. D. Wei, J. W. Kysar, and J. Hone, Science **321**, 385 (2008).
- [3] H. L. Cox, Brit J Appl Phys **3**, 72 (1952).
- [4] Y. Liu, B. Xie, Z. Zhang, Q. Zheng, and Z. Xu, J. Mech. Phys. Solids **60**, 591 (2012).
- [5] B. Chen, P. D. Wu, and H. Gao, Compos. Sci. Technol. **69**, 1160 (2009).
- [6] S. Park and K. Schulten, J. Chem. Phys. **120**, 5946 (2004).
- [7] S. Plimpton, J. Comput. Phys. **117**, 1 (1995).
- [8] S. Park, F. Khalili-Araghi, E. Tajkhorshid, and K. Schulten, J. Chem. Phys. **119**, 3559 (2003).
- [9] T. Zhang, X. Y. Li, S. Kadkhodaei, and H. J. Gao, Nano Lett. **12**, 4605 (2012).
- [10] W. Xia and S. Keten, J. Mater. Res. **30**, 36 (2015).
- [11] G. Jung, Z. Qin, and M. J. Buehler, Extreme Mech. Lett. **2**, 52 (2015).
- [12] G. Bell, Science **200**, 618 (1978).
- [13] S. Keten and M. J. Buehler, Nano Lett. **8**, 743 (2008).
- [14] S. Keten and M. J. Buehler, Phys. Rev. E **78**, 061913 (2008).